Journal of Power Sources 210 (2012) 116–121

Contents lists available at SciVerse ScienceDirect

Journal of Power Sources

journal homepage: www.elsevier.com/locate/jpowsour

Electrodeposition of Zn and Zn–Mn alloy coatings from an electrolytic bath prepared by recovery of exhausted zinc–carbon batteries

Paulo Sérgio da Silva[a,b,*], Edinéia P. Sartori Schmitz[a], Almir Spinelli[b], Jarem Raul Garcia[a]

[a] Departamento de Quimica, Universidade Estadual de Ponta Grossa, 84030-900 Ponta Grossa, PR, Brazil
[b] Departamento de Química, Universidade Federal de Santa Catarina, 88040-900 Florianópolis, SC, Brazil

ARTICLE INFO

Article history:
Received 2 December 2011
Received in revised form 7 March 2012
Accepted 9 March 2012
Available online 21 March 2012

Keywords:
Galvanic coatings
Zn–Mn alloy
Electrolytic bath
Recovery
Zinc–carbon batteries

ABSTRACT

The electrodeposition of galvanic coatings was performed using a chloride-based acidic electrolytic bath containing polyethylene glycol (PEG) as an additive. The electrolytic bath was prepared using Zn and Mn recovered from exhausted zinc–carbon batteries by means of acid leaching with HCl. The coatings were obtained potentiostatically at −1.2 V and −1.6 V (vs. Ag/AgCl) and galvanostatically with a current density of −10 mA cm^{-2}. The results indicated that the presence of PEG in the bath during galvanostatic deposition favored the formation of a coating containing a mixture of Zn and Zn–Mn alloy with an Mn content of around 2 wt%.

1. Introduction

Since the 1980s there has been a proliferation of electronic devices, such as radios, calculators, toys, cell phones, and many others, available on the market, which require low amounts of energy for their operation. Among the main energy sources used in these devices are the alkaline and zinc–carbon batteries, which are described as non-rechargeable or primary batteries [1]. Alkaline batteries make use of zinc powder as anode, a mixture of manganese dioxide and carbon as cathode and potassium hydroxide as the electrolyte. Already zinc–carbon batteries use a zinc cap as anode, a carbon rod with a mixture of manganese dioxide and carbon as cathode and ammonium chloride and/or zinc chloride as electrolyte. Thus, the spent primary batteries are composed essentially of C, Zn and MnO_2, as well as ZnO, MnOOH, Mn_2O_3 and Mn_3O_4 produced from the discharging reaction. However, small amounts of Hg, Pb and other heavy metals which are added to improve the performance of these devices can be present. Therefore, these batteries can become a source of hazardous environmental pollutants when disposed of in an inadequate way. The storage capacity of landfills and special waste disposal sites is limited, whereas is expected a rise in the worldwide demand for batteries driven by the increasing use of electrical and electronic products. In addition, the natural resources for the production of batteries are limited. So, the recovery of exhausted batteries will be increasingly important to both human health and the environment [1–5]. In recent years, several processes have been developed for the recycling of batteries in order to minimize the adverse environment impacts caused by their residues and to satisfy new regulations appearing around the world. Studies have reported the application of hydrometallurgical techniques using alkaline or acidic leaching as an efficient way to recover zinc and manganese from spent batteries. Hydrometallurgical techniques offer some benefits compared with pyrometallurgical methods, such as lower cost and no air pollution, as there are no particles produced. Furthermore, the metals present in the resulting leach liquor can be easily separated by precipitation or electrodeposition [3–10].

Electrodeposited coatings of zinc are extensively employed in the protection of steel against corrosion. However, this protective effect is not very effective under aggressive atmospheric conditions [11]. In recent years, several materials have been investigated to improve the durability of these coatings. Electrodeposited alloys of Zn, such as Zn–Ni, Zn–Co and Zn–Fe, present higher corrosion resistance than pure zinc coatings. Also, it has been reported in the literature that Zn–Mn alloys show even better corrosion resistance properties [12–15]. The high corrosion resistance of these alloys is likely due to the dual protective effect of manganese: on the one hand Mn dissolves first because it is thermodynamically less noble than Zn, thereby protecting Zn; and on the other hand Mn ensures the formation of compounds with a low solubility product over the galvanic coating. Depending on the aggressivity of the environment to which the Zn–Mn alloy is exposed, various compounds

* Corresponding author. Tel.: +55 48 3721 9778; fax: +55 48 3721 6850.
E-mail address: pssquimica@gmail.com (P.S. da Silva).

0378-7753
doi:10.1016/j.jpowsour.2012.03.021

may be found in the passive layer, including oxides such as MnO, MnO_2, Mn_5O_8 and γ-Mn_2O_3, or basic salts like $Zn_4(OH)_6SO_4{\cdot}xH_2O$ and $Zn_5(OH)_8Cl_2{\cdot}H_2O$ [12,16,17]. The protective effect of Zn–Mn is dependent on the Mn content of the alloy. Although it has been reported that among the Zn alloys those of Zn–Mn show the highest corrosion resistance, their deposition process presents some drawbacks related to the bath instability and current efficiency. Among the various electrolytic baths and additives proposed to obtain Zn–Mn alloys, the use of a chloride-based acid bath with polyethylene glycol (PEG) as the additive seems very promising [12–14].

The aim of this study was to recover zinc and manganese present in exhausted zinc–carbon batteries through chloride acidic leaching of the solid material. The leaching solution is then used as an electrolytic bath for the electrodeposition of the galvanic coating on AISI 1018 steel. Polyethylene glycol is used as the additive in the bath to obtain both Zn and Zn–Mn alloys.

2. Experimental details

The exhausted zinc–carbon batteries were dismantled manually followed by separation of their different parts: steel, plastic, paper, cap zinc, carbon rod and electrolytic paste (composed essentially of Zn, ZnO, MnO_2, MnOOH, Mn_2O_3, Mn_3O_4 and carbon). A sample of the electrolytic paste and anode scraps was dissolved in 0.5 mol L^{-1} HCl and 30% H_2O_2 (v/v). The role of hydrogen peroxide is to increase the leaching efficiency of manganese and hinder the oxidation of Mn^{2+} by the oxygen dissolved in the dissolution solution [4,9]. A proportion of 1.0 g of material to 30 mL of solution was used. The dissolution took 24 h under constant magnetic stirring at 298 K and the suspension was filtered under reduced pressure. The metallic ions present in the leach liquor were quantitatively determined by atomic absorption spectrometry (Varian model AA240FS). The pH of an aliquot of leach liquor was adjusted to 5.0 by addition of 10% KOH solution followed by the addition of 0.32 mol L^{-1} H_3BO_3. The resulting solution was named base solution S_0 after separation of the precipitates formed.

A study on the experimental conditions used for the deposition of the Zn and Zn–Mn alloy was carried out in a classical three-electrode cell. The working electrode was an AISI 1018 steel disk with a geometric area of 0.5 cm^2. Prior to each experiment, the working electrode was abraded with 600 grit emery paper and then rinsed with distilled water. A platinum sheet was used as the auxiliary electrode and $Ag/AgCl_{KClsat}$ was used as the reference electrode. The electrochemical experiments were carried out using a potentiostat/galvanostat (Autolab model PGSTAT100) coupled to a personal computer with specific data acquisition software installed.

The coating morphology was evaluated using scanning electron microscopy (SEM) coupled to an energy dispersive spectrometer (EDS) (Shimadzu model SSX-550). The identification of the deposited phases was carried out by X-ray diffraction (XRD) using a diffractometer (Shimadzu model XRD-6000).

3. Results and discussion

3.1. Characterization of the electrolytic bath

The quantitative analysis of the metal content in the electrolytic bath by atomic absorption spectrometry indicated that in addition to Zn^{2+} and Mn^{2+} traces of other species such as Fe^{2+}, Cu^{2+} and Pb^{2+} were present in solution. When the pH of the solution was adjusted to 5.0 precipitation of some metallic ions occurred. The analysis of leach liquor after separation of the precipitates by atomic absorption spectrometry indicated only the presence of Zn^{2+} and Mn^{2+}, in the concentrations of 0.1 mol L^{-1} and 0.06 mol L^{-1}, respectively. Boric acid (H_3BO_3) was then added and this solution was used as the base solution (S_0). Boric acid was used because it inhibits both hydrogen formation and zinc deposition by acting as a buffer, limiting the hydrogen evolution at the electrode surface during electrodeposition [13,14]. Table 1 shows the composition of the leach liquor and the parameters used in the electrodeposition steps.

Table 1
Composition of the leach liquor and electrodeposition parameters.

Composition	
Zn^{2+}	0.1 mol L^{-1}
Mn^{2+}	0.06 mol L^{-1}
H_3BO_3	0.32 mol L^{-1}
PEG	Without (S_0) or 1 g L^{-1} (S_1)
Parameters	
Deposition potential	−1.2 and −1.6 V/(Ag/AgCl)
Applied current density	−10 mA cm^{-2}
Time	15 min
Temperature	25 °C (±2 °C)
Solution	Unstirred

3.2. Potentiostatic electrodeposition

The conditions used during the potentiostatic electrodeposition using the S_0 and S_1 solutions were chosen in agreement with previous studies carried out by other authors on the electrodeposition of Zn–Mn alloys [12]. The resulting current–time curves are shown in Fig. 1. At −1.2 V, in the absence of additive, the current density stabilized at around −4.5 mA cm^{-2}. In the presence of PEG, the current density is slightly less negative (−3.6 mA cm^{-2}). When electrodeposition was carried out at −1.6 V the current densities with and without the additive were −17.6 mA cm^{-2} and −10.8 mA cm^{-2}, respectively. It is important to note that the presence of additive during the electrodeposition at more negative potentials makes the current density more stable. The instability observed in the electrodepositions carried out with S_0 solution, particularly at −1.6 V, may be attributed to hydrogen evolution. In a study on the effect of additives on the hydrogen evolution reaction during Zn electrodeposition, Song et al. [18] suggested that PEG acts as an inhibitor of hydrogen absorption in the electrodeposited Zn.

3.3. Characterization of the coatings obtained by potentiostatic deposition at −1.2 V

Fig. 2 shows the morphology of the deposit obtained potentiostatically at −1.2 V from the base solution (S_0). The SEM image

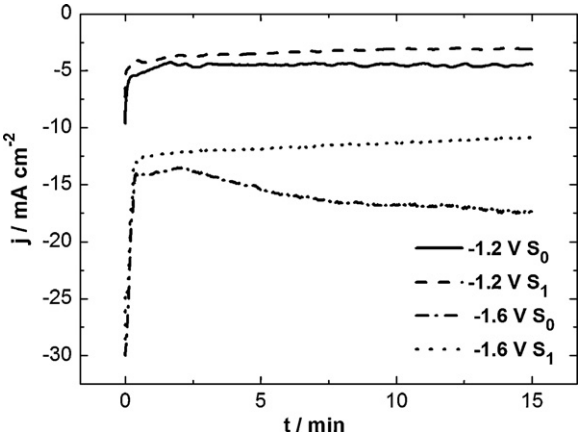

Fig. 1. Potentiostatic curves obtained during electrodeposition onto an AISI 1018 steel electrode from S_0 and S_1 solutions.

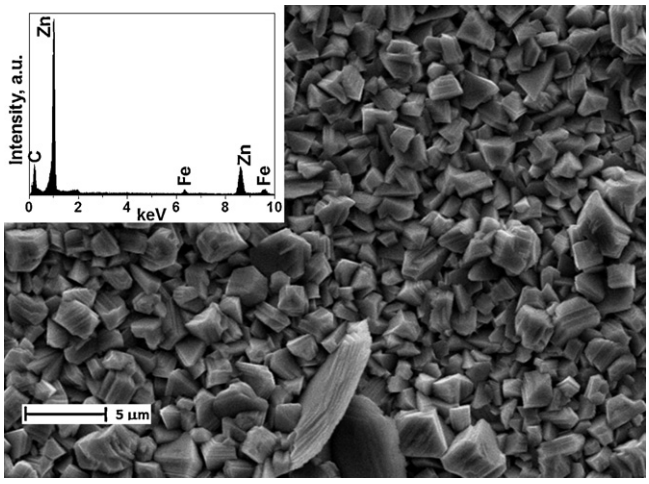

Fig. 2. SEM image of the deposit formed on AISI 1018 steel electrode at −1.2 V/(Ag/AgCl), t = 15 min, from solution S_0. The results for the EDS analysis are shown in the inset.

shows that the deposit comprises hexagonal plates with pyramidal clusters grouped into nodules of several sizes, as is normal for pure zinc electrodeposits [18]. The EDS analysis (inset in Fig. 2) showed the presence of zinc as the predominant element in the coating. In the presence of PEG, the deposit obtained comprises hexagonal crystals oriented perpendicularly to the substrate surface (Fig. 3) and the zinc also was the predominant element (inset in Fig. 3). This type of morphology was also observed by Ballesteros et al. [11] who studied the influence of PEG as an additive on the mechanism of Zn deposition and nucleation. Although differences were observed in the morphology of the deposits obtained with and without the use of the additive, the XRD analysis (Fig. 4) showed similar composition of both deposits. As can be seen, the formation of a Zn–Mn alloy could not be obtained from potentiostatic experiments carried out at −1.2 V.

3.4. Characterization of the coatings obtained by potentiostatic deposition at −1.6 V

Fig. 5 shows the morphology of the deposit obtained potentiostatically at −1.6 V without the use of the additive. In the SEM image an amorphous and porous deposit covering some parts of the

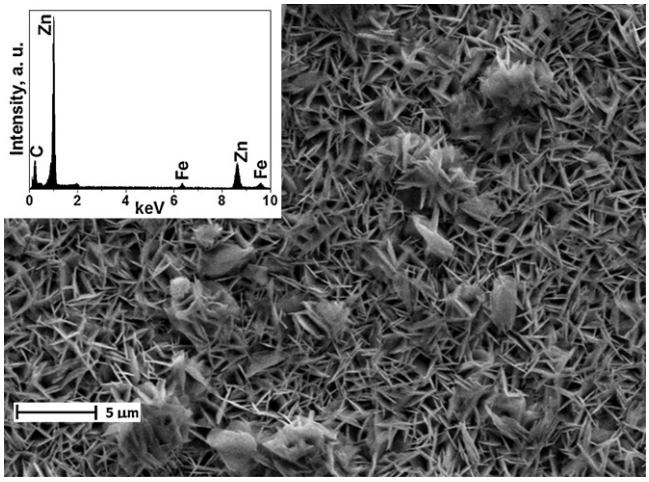

Fig. 3. SEM image of the deposit formed on AISI 1018 steel electrode at −1.2 V/(Ag/AgCl), t = 15 min, from solution S_1. The results for the EDS analysis are shown in the inset.

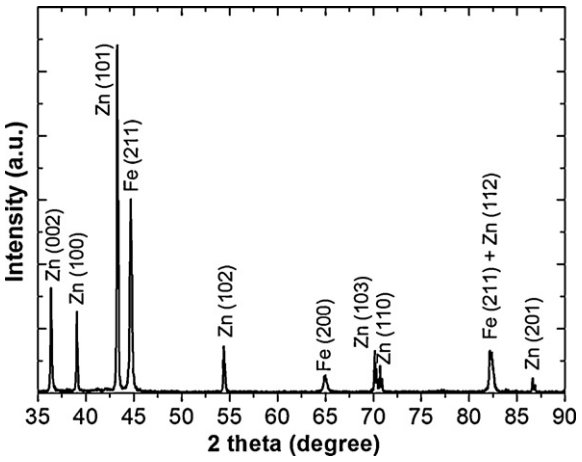

Fig. 4. X-ray diffraction (XRD) pattern of the deposit obtained on AISI 1018 steel electrode at −1.2 V/(Ag/AgCl), t = 15 min.

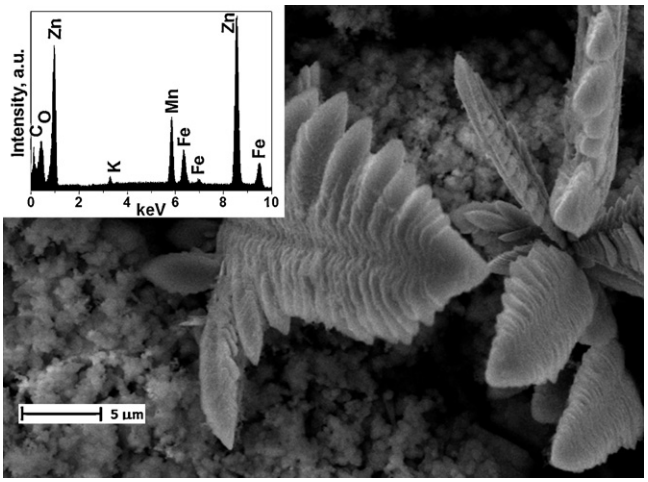

Fig. 5. SEM image of the deposit formed on AISI 1018 steel electrode at −1.6 V/(Ag/AgCl), t = 15 min, from solution S_0. The results for the EDS analysis are shown in the inset.

substrate can be observed. The EDS analysis (inset in Fig. 5) indicated that the manganese content of this deposit is around 8 wt%.

The XRD analysis (Fig. 6) also indicated that these experimental conditions did not favor the formation of a Zn–Mn alloy. This

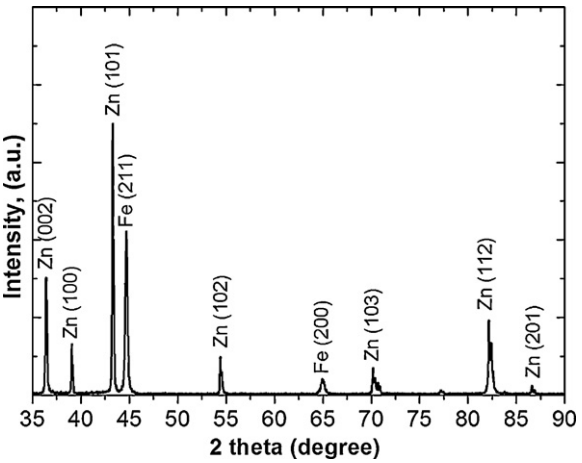

Fig. 6. X-ray diffraction (XRD) pattern of a deposit obtained on AISI 1018 steel electrode at −1.6 V/(Ag/AgCl), t = 15 min, from solution S_0.

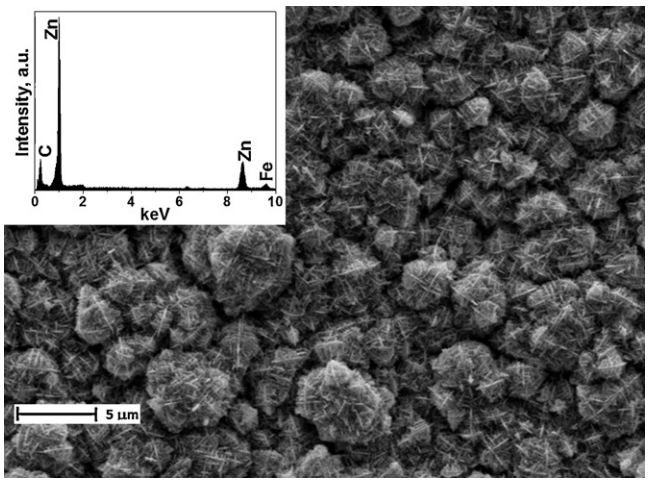

Fig. 7. SEM image of the deposit formed on AISI 1018 steel electrode at −1.6 V/(Ag/AgCl), t = 15 min, from solution S_1. The results for the EDS analysis are shown in the inset.

result may be related to the formation of $Mn(OH)_{2(s)}$ species on the substrate surface due to the hydrogen formation under these experimental conditions, resulting in an increase in the pH in the vicinity of the working electrode [19]. In addition, the formation of $Mn(OH)_2$ in high alkaline conditions agrees well with the Eh × pH (Pourbaix) diagrams [20].

In comparison with the morphology observed for the deposit obtained without PEG, the deposit formed in the presence of the additive is very different. The SEM image and EDS analysis (Fig. 7) show that the deposit formed is compact and homogenous with a cauliflower-like morphology; however, once again, the presence of manganese in the deposit could not be detected. The change in the morphology of the deposit may be associated with the partial adsorption of the additive on the electrode surface during the electrodeposition of Zn^{2+} [21]. In addition, the XRD analysis (Fig. 8) revealed that the deposit comprises principally Zn crystals in the plane (1 0 1), corroborating the EDS results.

3.5. Galvanostatic electrodeposition

As the current density stabilized at around −10 mA cm^{-2} with the presence of PEG in the electrolytic bath during potentiostatic electrodeposition at −1.6 V, this current density was chosen for the attempted galvanostatic electrodeposition of the Zn–Mn alloy.

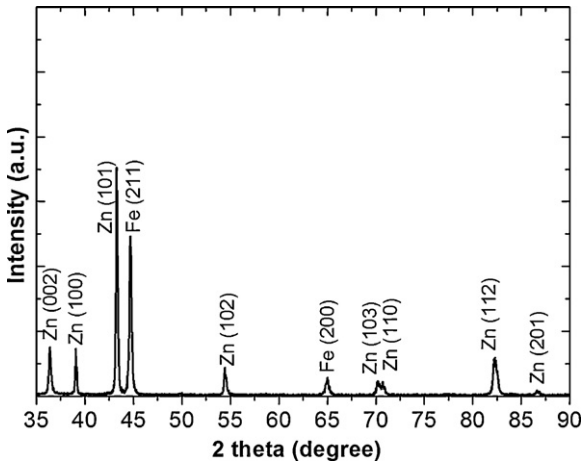

Fig. 8. X-ray diffraction (XRD) pattern of a deposit obtained on AISI 1018 steel electrode at −1.6 V/(Ag/AgCl), t = 15 min, from solution S_1.

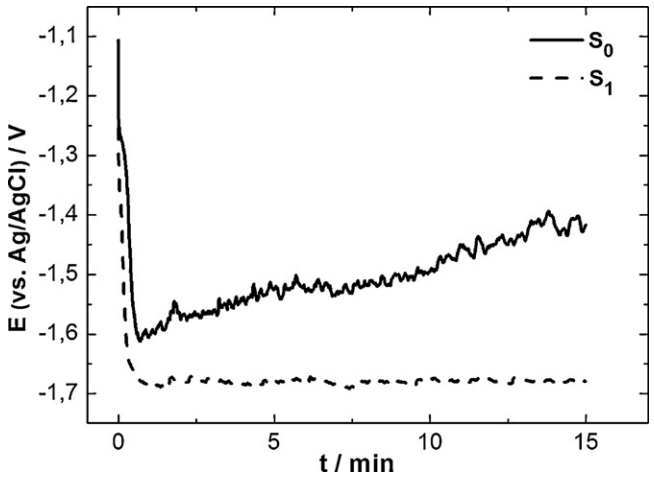

Fig. 9. Chronopotentiometric curves obtained during electrodeposition of the deposits on AISI 1018 steel electrode from base solution S_0 and solution S_1.

Fig. 9 shows the chronopotentiometric curves obtained. In the absence of PEG the potential changed during the electrodeposition, resulting in a rough and irregular deposit, as evidenced in the SEM analysis. On the other hand, when the additive was added to the base solution, the deposition potential stabilized at around −1.68 V at the beginning of the electrodeposition. Additives such as PEG can shift the potential of Zn deposition to more negative values, enabling Zn alloys to be obtained with metals for which the deposition potentials are very negative [11]. In addition, the use of PEG as an additive allowed a compact and homogenous deposit to be obtained, as discussed in Section 3.6.

3.6. Characterization of the coatings obtained galvanostatically

Fig. 10 shows the SEM image of the deposit obtained galvanostatically at −10 mA cm^{-2} in the absence of PEG. The deposit formed is porous and with grains of diverse dimensions irregularly distributed on the substrate surface. The EDS analysis (inset in Fig. 10) revealed that there is no manganese present in the coating. In addition, the XRD patterns were the same as those obtained during the potentiostatic deposition at −1.2 V (see Section 3.3) indicating only the presence of the Zn crystals in different planes. The results obtained in the presence of PEG indicated the formation

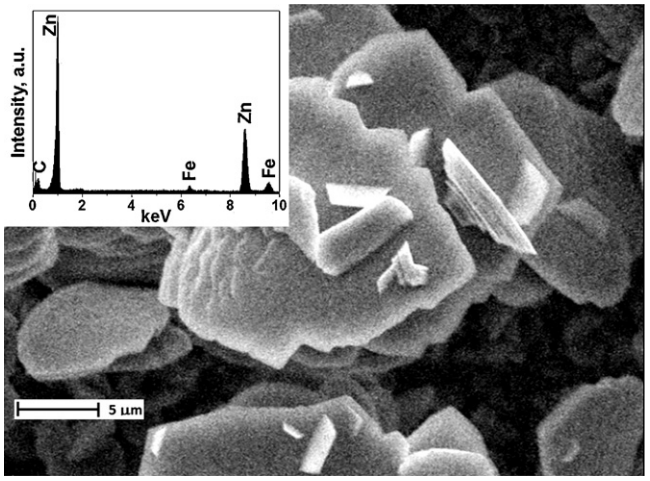

Fig. 10. SEM image of the deposit formed on AISI 1018 steel electrode at −10 mA cm^{-2}, t = 15 min, from solution S_0. The results for the EDS analysis are shown in the inset.

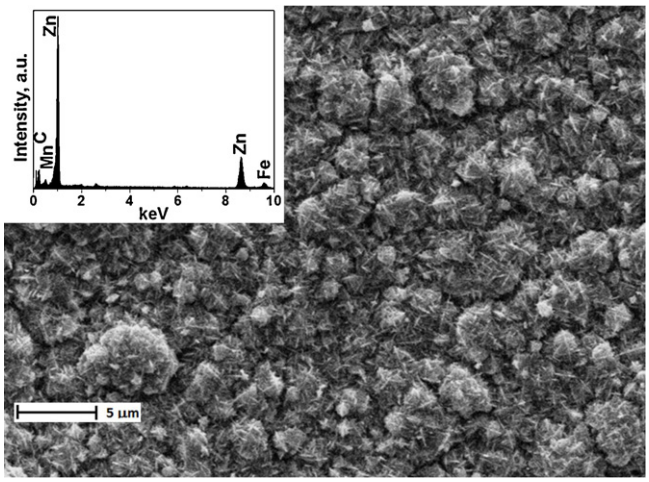

Fig. 11. SEM image of the deposit formed on AISI 1018 steel electrode at $-10\,mA\,cm^{-2}$, $t = 15$ min, from solution S_1. The results for the EDS analysis are shown in the inset.

of the Zn–Mn alloy during galvanostatic electrodeposition. Fig. 11 shows the SEM micrograph of the deposit obtained under these conditions. The results indicate that the PEG decreased the mean size of grains inducing the formation of a smooth deposit. Although the EDS analysis did not clearly indicate the presence of Mn in the deposit, the XRD results (Fig. 12) showed a diffractogram characteristic of a mixture of Zn and ε-phase Zn–Mn with different crystallographs.

This finding may be related to the low manganese content, around 2 wt% in the deposit. Ballesteros et al. [11] have reported that the presence of additives such as PEG can shift the potential of Zn deposition to very negative values. Such behavior is associated with the partial adsorption of PEG onto the substrate surface. The authors related that in the presence of this additive the electrodeposition of zinc can occur in two different ways. First, the zinc is electrodeposited onto the active sites on the electrode surface that are not blocked by adsorbed PEG molecules. In second, the zinc is electrodeposited onto the active sites that are liberated when PEG molecules are desorbed from electrode surface. This occurs in much more negative potential than the first. The effect of displacement of the zinc reduction potential to more negative values is known as cathodic polarization. Accordingly, potentials as negative as -1.6 V (SCE) could be used to obtain deposits of zinc alloys with metals such as Mn. Similar XRD results were observed by Sylla

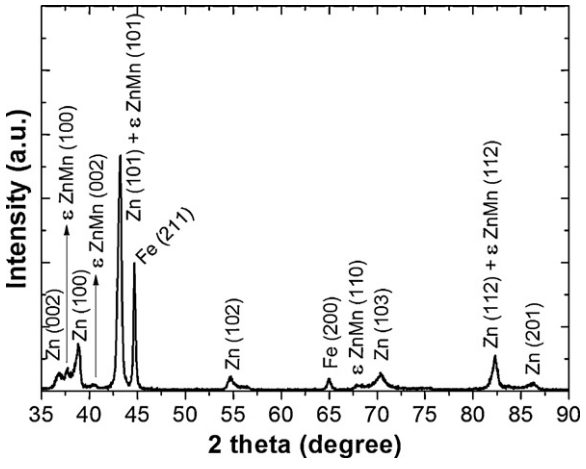

Fig. 12. X-ray diffraction (XRD) pattern of a deposit obtained on AISI 1018 steel electrode at $-10\,mA\,cm^{-2}$, $t = 15$ min from solution S_1.

Table 2
Electrodeposition parameters and characteristics of the deposits obtained.

	Deposit
Without additive	
−1.2 V	Homogenous, comprised by hexagonal plates, only Zn
−1.6 V	Amorphous and porous, Zn and $Mn(OH)_2$ (~8 wt% Mn)
$-10\,mA\,cm^{-2}$	Amorphous and porous, only Zn
With additive	
−1.2 V	Homogenous, comprised by hexagonal crystals, only Zn
−1.6 V	Homogenous, cauliflower morphology, only Zn
$-10\,mA\,cm^{-2}$	Homogenous, smooth, Zn and Zn–Mn alloys (~2 wt% Mn)

et al. [13]. They reported an Mn content of 1 wt% in a Zn–Mn alloy deposit obtained from a chloride-based acidic bath containing PEG as an additive. The authors postulated that the presence of PEG allowed the formation of a compact and homogenous deposit with cauliflower-like morphology. However, the presence of PEG in the solution hindered manganese deposition and inhibited the formation of the ζ phase Zn–Mn. It is important to note that the peaks observed in our study for Zn and the phases of Zn–Mn alloy are very close and some overlap may have occurred. Table 2 shows a summary of all parameters used in the electrodeposition and some characteristics of the deposits obtained.

4. Conclusions

The results reported herein demonstrate that it is possible to obtain galvanic coatings in a bath prepared from zinc and manganese recovered from exhausted zinc–carbon batteries. The presence of polyethylene glycol as an additive in the electrolytic bath during galvanostatic deposition favors the obtainment of a compact and homogenous deposit containing a mixture of Zn and a Zn–Mn alloy, with a manganese content around 2 wt%.

The proposed method may represent an alternative use for zinc and manganese recovered from exhausted alkaline and zinc–carbon batteries and thus minimize the adverse environment impacts caused by these residues.

Acknowledgments

The authors are grateful for the financial assistance provided by CNPq and Fundação Araucária (Brazil).

References

[1] R.G. da Silva, C.N. da Silva, J.C. Afonso, Quím. Nova 33 (9) (2010) 1957–1961.
[2] E. Sayilgan, T. Kukrer, G. Civelekoglu, F. Ferella, A. Akcil, F. Veglio, M. Kitis, Hydrometallurgy 97 (2009) 158–166.
[3] E. Sayilgan, T. Kukrer, N.O. Yigit, G. Civelekoglu, M. Kitis, J. Hazard. Mater. 173 (2010) 137–143.
[4] G. Senanayake, S.-M. Shin, A. Senaputra, A. Winn, D. Pugaev, J. Avraamides, J.-S. Sohn, D.-J. Kim, Hydrometallurgy 105 (2010) 36–41.
[5] A.L. Salgado, A.M.O. Veloso, A.M. Andrade, D.D. Pereira, A. Salum, M.B. Mansur, J. Power Sources 115 (2003) 367–373.
[6] L.R.S. Veloso, L.E.O.C. Rodrigues, D.A. Ferreira, F.S. Magalhaes, M.B. Mansur, J. Power Sources 152 (2005) 295–302.
[7] M.B.J.G. Freitas, M.K. de Pietre, J. Power Sources 128 (2004) 343–349.
[8] M.B.J.G. Freitas, M.K. de Pietre, J. Power Sources 143 (2005) 270–274.
[9] M.B.J.G. Freitas, V.C. Pegoretti, M.K. Pietre, J. Power Sources 164 (2007) 947–952.
[10] I. De Michelis, F. Ferella, E. Karakaya, F. Beolchini, F. Veglio, J. Power Sources 172 (2007) 975–983.
[11] J.C. Ballesteros, P. Díaz-Arista, Y. Meas, R. Ortega, G. Trejo, Electrochim. Acta 52 (2007) 3686–3696.
[12] P. Díaz-Arista, Z.I. Ortiz, H. Ruiz, R. Ortega, Y. Meas, G. Trejo, Surf. Coat. Technol. 203 (2009) 1167–1175.
[13] D. Sylla, J. Creus, C. Savall, O. Roggy, M. Gadouleau, Ph. Refait, Thin Solid Films 424 (2003) 171.
[14] C. Savall, C. Rebere, D. Sylla, M. Gadouleau, Ph. Refait, J. Creus, Mater. Sci. Eng. A 430 (2006) 165.
[15] M. Bučko, J. Rogan, S.I. Stevanović, A. Perić-Grujić, J.B. Bajat, Corros. Sci. 53 (2011) 2861–2871.

[16] Z.I. Ortiz, P. Díaz-Arista, Y. Meas, R. Ortega-Borges, G. Trejo, Corros. Sci. 51 (2009) 2703–2715.
[17] A. Gomes, M.I. da Silva Pereira, Electrochim. Acta 51 (2006) 1342–1350.
[18] K.D. Song, K.B. Kim, S.H. Han, H. Lee, Electrochem. Solid-State Lett. 7 (2) (2004) C20–C24.
[19] P. Díaz-Arista, R. Antaño-López, Y. Meas, R. Ortega, E. Chainet, P. Ozil, G. Trejo, Electrochim. Acta 51 (2006) 4393.
[20] Atlas of Eh–pH diagrams. Intercomparison of Thermodynamic Databases, Geological Survey of Japan Open File Report No. 419, National Institute of Advanced Industrial Science and Technology, May 2005. Available via www.gsj.jp/GDB/openfile/files/no0419/openfile419e.pdf. Accessed March 6th, 2012.
[21] J.W. Kim, J.Y. Lee, S.M. Park, Langmuir 20 (2004) 459–466.